Chemical trend of the formation energies of the group-III and group-V dopants in Si quantum dots

Jie Ma and Su-Huai Wei

The chemical trend of the formation energies of group-III and group-V dopants in Si quantum dots

Jie Ma and Su-Huai Wei

National Renewable Energy Laboratory, Golden, Colorado 80401, USA

Doping behavior in quantum dots (QDs) differs from that in the bulk. Despite many efforts, the doping properties are still not fully understood. Using first-principles methods, we have calculated the formation energies of various group-III acceptors and group-V donors doping at all non-equivalent sites in a Si QD ($Si_{147}H_{100}$). To analyze the trend of the formation energy, we decompose it into two terms: the unrelaxed formation energy (chemical energy) and the relaxation energy. We find that the unrelaxed formation energy generally increases as the dopant moves from the center of the QD to the surface. The variation of the unrelaxed formation energy in the surface region is explained by the variation of the local potential of the QD and the size effect. The relaxation energy gain increases as the size mismatch between the dopant and Si atom increases. Generally, the relaxation effect becomes more significant as the dopant moves toward the surface of the QD. The trend of the formation energy is determined by the two terms discussed above. If the size mismatch between the dopant and Si atom is small, the trend of the formation energy generally follows that of the unrelaxed formation energy, increasing as the dopant moves from the center to the surface; thus, these dopants have a better chance of staying in the core region. On the other hand, if the size mismatch is large, the relaxation effect dominates and the formation energy decreases, which indicates these dopants cannot enter the core region under equilibrium growth conditions.

I. INTRODUCTION

Doping is one of the most important issues in semiconductor physics.[1,2] The charge carrier generated by doping can profoundly change the properties of semiconductors and their performance in optoelectronic devices.[3–7] Semiconductor nanocrystals have great potential in applications such as light-emitting diodes, lasers, solar cells, and biomedical labeling reagents, because their physical properties, such as band gaps and optical transitions, can be tailored continuously by controlling their size or shape.[8–11] As in bulk semiconductors, doping is required for applications in QDs. For example, ZnS and ZnSe nanocrystals can have intense photoluminescence emission over a wide range of wavelength after doped with Cu or Mn.[12,13] In CdSe nanocrystals, a few Ag atoms per nanocrystal causes a large enhancement in the fluorescence, but more Ag atoms decrease the intensity from its maximum.[14]

Silicon (Si) is one of the most important semiconductors for microelectronic and energy applications, and Si quantum dots (QDs) have also attracted many attentions.[15–23] Experimentally, free-standing Si QDs have been synthesized in either liquid phase or gas phase.[24–28] Gas-phase doping of P and B in these free-standing Si QDs with at least partial hydrogen coverage of their surface has also been achieved by introducing dopant precursors (diborane and phosphine) into the plasma.[29] Although the doping in bulk Si have been widely studied before, as the size of the semiconductor approaches nano dimensions, the doping properties could be very different from those in the bulk system. These defect properties, such as the location of dopants in QDs, are still open questions. Theoretically, there were many studies on the defect properties in Si QDs.[30–36] In most of these studies, the doping at the center site of the QD has been discussed. It is now clear that due to the quantum confinement effect,[37] doping at the center site of the QD becomes energetically more difficult (i.e., the formation energy and ionization energy of the defect increase) as the QD decreases in size.[30–35] In bulk Si, all the Si atoms are equivalent, so there is only one doping site for an isolated dopant. However, in a QD, there are many non-equivalent doping sites due to the existence of the surface. Although several groups have studied doping at other sites, in those studies doping has been calculated only along one or two paths.[31,32,36] Because there are many more possible paths in a QD, a more comprehensive understanding of doping in the whole QD is still lacking.

In this paper, we present a comprehensive study of the doping properties of the whole QD. The QD is built by including all atoms within a given radius centered at a lattice site. At the surface, atoms with more than two dangling bonds are removed and the remaining surface dangling bonds of the QD are passivated with hydrogen (H). As the size effect of the QD has been well discussed before,[32] we study only one QD: $Si_{147}H_{100}$. In principle, we have to calculate doping at every site in the QD, which is of course time consuming. Fortunately, the QD we built has T_d symmetry. It is obvious that symmetry-related sites have the same properties. Therefore, we need only consider the non-equivalent sites. In this study, we will not consider dopants substituting surface atoms that are directly connected to the passivating agents (H atoms are used here), so there are in total 8 non-equivalent sites in our model. Of course, in a larger QD there are more non-equivalent sites, but the trend of the doping properties should be similar. We have calculated the formation energies of various group-III and group-V dopants at every non-equivalent site. We find that the unrelaxed formation energy and the relaxation energy generally have opposite trends. The variation of the unrelaxed formation energy in the surface region is explained by the local potential and the size effect of the QD host. If the dopant size mismatch is small, the unrelaxed formation energy dominates and the formation energy generally increases as the dopant moves away from the center, which indicates these dopants may stay in the core region. If the size mismatch is large, the relaxation effect dominates and the formation energy decreases as the dopant moves from the center to the surface, which indicates these dopants prefer to be in the surface region. The same variation in the unrelaxed formation energy in the surface region still exists in the formation energy, which affects the most stable doping site of the dopant. Similar formation energy trends have also been observed in Si nanowires.[38–40] Because of the similarity between Si QDs and nanowires, our explanations on the trends of the formation energy may also be applied to free-standing hydrogen passivated Si nanowires.

II. METHODS

Our calculations are based on density functional theory (DFT) within the local density approximation (LDA)[41] as implemented in VASP code.[42] The projector augmented wave (PAW) pseudopotentials[43] are employed and the valence wavefunctions are expanded in a plane wave basis with an energy cutoff of 300 eV. Because we are calculating free-standing QDs, only the Gamma point is used in Brillouin zone integration. The vacuum is around 10 Å. We have also tested larger energy cutoff and vacuum size, and the change of formation energy is negligible. In the relaxation, all the atoms are allowed to move until the force on every atom is smaller than 0.02 eV/Å.

The formation energy of a dopant α is defined as

$$\Delta E(\alpha) = E(\alpha) - E(\text{host}) - \mu_\alpha + \mu_{\text{Si}} \tag{1}$$

$E(\alpha)$ is the calculated total energy for the system containing the dopant α, and $E(\text{host})$ is the calculated total energy for the undoped Si QD host. μ_α and μ_{Si} are the chemical potentials of the dopant α and Si atom. Here we employ their element solid values. We want to point out that the choice of chemical potentials does not affect the calculated trends at all.

III. RESULTS AND DISCUSSIONS

The structure of the undoped Si QD is presented in Fig. 1, including the charge densities of the highest occupied molecular orbital (HOMO) and the lowest unoccupied molecular orbital (LUMO). Generally, the atoms around the surface feel a stronger quantum confinement effect, so the bonding-antibonding splitting is larger in the surface region than that in the center region. Therefore, the charge densities of both the HOMO and LUMO are located at the center of the QD. The lengths of the Si-Si bonds are not all the same in the QD. The average bond length of the four Si-Si bonds at every non-equivalent site is presented in Fig. 2. The bond length at the center of the QD is 2.338 Å, which is the same as the bond length in bulk Si. However, the average bond lengths for the sites close to the surface show some variation due to the surface effect. Similarly, the local potential (the potential a test electron feels at the position of the Si nuclei in the undoped Si QD) at these sites also shows some variation (Fig. 3), which indicates some charge redistribution due to the surface effect. From the average bond length and the local potential, we notice that the variation at the first four sites is rather small compared to the last four sites, which indicates the surface effects are negligible around the core region. However, the last four sites show large surface-induced variation, although they do not connect directly to the passivating H atoms at the surface. These variations of the host near the surface affect the doping properties, as will be shown below.

To analyze the doping properties, we decompose the formation energy of the dopants into two physically recognizable terms. First, we neglect the relaxation around the dopant and calculate the unrelaxed formation energy. In this step, the chemical effect of the dopant is included. Second, we relax the internal structural freedom and calculate the relaxation energy. In this step, the strain energy induced by the dopant is released. The formation energy is the sum of these two terms.

We first consider the unrelaxed formation energy. We have calculated the unrelaxed formation energies of various group-III acceptors and group-V donors at every non-equivalent site of the QD, and the results are presented in Fig. 4. The overall trend shows that as the doping site moves away from the center of the QD, the unrelaxed formation energy increases for all the dopants. This can be understood as follows. The wavefunction of the defect level is localized on the dopant site and derived from the bonding state (acceptor) or antibonding state (donor).[6] As the bonding state energy decreases or the antibonding state energy increases, it costs more energy to create holes at the acceptor level or add electrons to the donor level, so the formation energy will increase.[32,44] As we discussed earlier, as the atom moves away from the center, the bonding-antibonding splitting increases, so the bonding state energy decreases, which increases the acceptor formation energy, and the antibonding state energy increases, which increases the donor formation energy. Moreover, as the dopant moves away from the center of the QD, the defect electron (or hole) deviates from the dopant ion and therefore the Coulomb attraction between the defect electron (or hole) and the dopant ion decreases, which also contributes to the increase of the unrelaxed formation energy.[33]

At the first four sites (core region), the unrelaxed formation energies of the larger dopants increase more slowly than those of the smaller dopants. This is related to the trend of the bond length in the host (Fig. 2). We notice that in the core region the bond length increases as the site moves away from the center. For large dopants, the strain energy cost decreases at the site with a larger bond length, and therefore the unrelaxed formation energies increase more slowly. On the other hand, for small dopants, the strain energy cost increases at the site with a larger bond length, and therefore the unrelaxed formation energies increase even faster. The bond length of the fourth site is the largest, and we observe a dip in the unrelaxed formation energy curves of the large dopants (Al, In, Sb, and Bi). At the last four sites (surface region), the unrelaxed formation energy shows some variation. This is related to the local potential of the host (Fig. 3). Due to the distribution of the defect wavefunction, the acceptor always carries some negative charge and the donor carries some positive charge, even in the neutral state. The unrelaxed formation energies of these dopants are affected by the local potential. For the acceptor, the unrelaxed formation energy should increase as the local potential increases. Therefore, the unrelaxed formation energies of Al, Ga, and In follow the same variation as the local potential. For the donor, the unrelaxed formation energy should decrease as the local potential increases. Therefore, the unrelaxed formation energies of N, P, and As exhibit the opposite variation. However, the smallest acceptor B and the largest donors Sb and Bi do not follow this trend. This is because, as the size mismatch between the dopant and Si atom becomes very large, the size effect also plays an important role. As we have discussed above, the energy of the small dopant increases as the bond length increases, and that of the large dopant decreases as the bond length increases. If the size effect dominates, the small dopant tends to follow the same variation trend as the bond length (Fig. 2), whereas the large dopant tends to do the opposite. At the last four

non-equivalent sites, the average bond length and the local potential actually exhibit opposite variations. For the large acceptor or small donor, the local potential and the average bond length have the same effect on the variation of the unrelaxed formation energy, but for the small acceptor or large donor, they have opposite effects. Therefore, as the size of the acceptor increases or the size of the donor decreases, the variation of the unrelaxed formation energy does not change. However, as the size of the acceptor decreases or the size of the donor increases, the variation of the unrelaxed formation energy will change, which explains the different behavior of B, Sb, and Bi in the surface region.

Next, we look at the relaxation energy. The relaxation of the atoms around the dopant lowers the total energy. The relaxation energies of various group-III acceptors and group-V donors are presented in Fig. 5. For dopants that have large size mismatch with Si, such as B, In, N, Sb, and Bi, the relaxation energy gain is relatively large due to the release of the strain energy. For a dopant, the relaxation energy gain becomes larger as it moves closer to the surface of the Si QD, because the strain can be more easily released at the surface. Overall, the unrelaxed formation energy and the relaxation energy exhibit opposite trends as a dopant moves from the center to the surface of the QD.

The formation energy is the sum of the unrelaxed formation energy and the relaxation energy, which is presented in Fig. 6. Because the two terms have opposite effects on the formation energy, the competition between them determines the trend of the formation energy. For dopants that have small size mismatch with Si, the unrelaxed formation energy dominates, and therefore the formation energy increases as the dopant moves from the center to the surface region. These dopants have better chances to enter the core region of the QD under equilibrium conditions. For dopants that have large size mismatch with Si, the relaxation energy dominates, and therefore the formation energy decreases as the dopant moves from the center to the surface region. These dopants cannot enter the core region and will stay near the surface of the QD under equilibrium conditions. We can also observe the same variation in the formation energy as that in the unrelaxed formation energy. For some dopants, the variation in the formation energy is large enough to modify the trend of the formation energy. The most stable site of these dopants is neither the center nor the surface and is actually determined by the variation that we explained above.

IV. SUMMARY

In summary, we have calculated the formation energies of various group-III acceptors and group-V donors at all the non-equivalent sites in a Si QD. We decompose the formation energy into two terms: the unrelaxed formation energy and the relaxation energy. We find that the unrelaxed formation energy generally increases as the dopant moves away from the center of a Si QD, whereas the relaxation energy decreases. The trend of the formation energy is determined by the competition between the two terms. For the dopants with small size mismatch, the formation energy increases as the dopant moves from the center to the surface, which indicates these dopants may exist in the core region; for the dopants with large size mismatch, the formation energy decreases as the dopant moves from the center to the surface, which indicates these dopants can only stay in the surface region. In the surface region, there is some variation in the formation energy due to the local potential effect and the size effect of the host. The most stable site of the dopant is affected by the variation near the surface. Similar formation energy trends have also been observed in Si nanowires.[38–40] Because of the similarity between Si QDs and nanowires, our explanations on the trends of the formation energy may also be applied to free-standing hydrogen passivated Si nanowires.

[1] S. M. Sze, *Physics of Semiconductors Devices* (Wiley, New York, 1981).

[2] A. S. Grove, *Physics and Technology of Semiconductor Devices* (Wiley, New York, 1967).

[3] B. G. Streetman and S. Banerjee, *Solid State Electronic Devices* (Prentice Hall, New Jersey, 2000), 5th ed.

[4] P. M. Voyles, D. A. Muller, J. L. Grazul, P. H. Citrin, and H. J. L. Gossmann, Nature (London) **416**, 826 (2002).

[5] D. J. Chadi, P. H. Citrin, C. H. Park, D. L. Adler, M. A. Marcus, and H. J. Gossmann, Phys. Rev. Lett. **79**, 4834 (1997).

[6] S.-H. Wei, Comp. Mater. Sci. **30**, 337 (2004).

[7] G. F. Neumark, Mater. Sci. Eng. R **21**, 1 (1997).

[8] A. P. Alivisatos, Science **271**, 933 (1996).

[9] L. Manna, E. Scher, and A. P. Alivisatos, J. Am. Chem. Soc **122**, 12700 (2000).

[10] X. Peng, L. Manna, W. D. Yang, J. Wickham, E. Scher, A. Kadavanich, and A. P. Alivisatos, Nature **404**, 59 (2000).

[11] J. Heitmann, F. Muller, M. Zacharias, and U. Gosele, Adv. Mater. **17**, 795 (2005).

[12] N. Pradhan, D. M. Battaglia, Y. Liu, and X. Peng, Nano Lett. **7**, 312 (2007).

[13] N. S. Karan, D. D. Sarma, R. M. Kadam, and N. Pradhan, J. Phys. Chem. Lett. **1**, 2863 (2010).

[14] A. Sahu, M. S. Kang, A. Kompch, C. Notthoff, A. W. Wills, D. Deng, M. Winterer, C. D. Frisbie, and D. J. Norris, Nano Lett. **12**, 2587 (2012).

[15] A. J. Nozik, M. C. Beard, J. M. Luther, M. Law, R. J. Ellingson, and J. C. Johnson, Chem. Rev. **110**, 6873 (2010).

[16] M. C. Beard, K. P. Knutsen, P. Yu, J. M. Luther, Q. Song, W. K. Metzger, R. J. Ellingson, and A. J. Nozik, Nano Lett. **7**, 2506 (2007).

[17] B. B. Smith and A. J. Nozik, Nano Lett. **1**, 36 (2001).

[18] M. Koshida and N. Matsumoto, Mater. Sci. Eng. R **40**, 169 (2003).

[19] L. Brus, J. Phys. Chem. **98**, 3575 (1994).

[20] L. E. Brus, P. F. Szajowski, W. L. Wilson, T. D. Harris, S. Schuppler, and P. H. Citrin, J. Am. Chem. Soc. **117**, 2915 (1995).

[21] V. A. Belyakov, V. A. Burdov, R. Lockwood, and A. Meldrum, Advances in Optical Technologies **2008**, 279502 (2008).

[22] Z. Zhou, R. A. Friesner, and L. Brus, J Am. Chem. Soc. **125**, 15599 (2003).

[23] Z. Zhou, L. Brus, and R. A. Friesner, Nano Lett. **3**, 163 (2003).

[24] R. K. Baldwin, J. Zou, K. A. Pettigrew, G. J. Yeagle, R. D. Britt, and S. M. Kauzlarich, Chem. Commun. **0**, 658 (2006).

[25] L. Mangolini, E. Thimsen, and U. Kortshagen, Nano Lett. **5**, 655 (2005).

[26] L. Mangolini and U. Kortshagen, Adv. Mater. **19**, 2513 (2007).

[27] X. D. Pi, R. W. Liptak, S. A. Campbell, and U. Kortshagen, Appl. Phys. Lett. **91**, 083112 (2007).

[28] Y.-C. Liao and J. T. Roberts, J. Am. Chem. Soc. **128**, 9061 (2006).

[29] X. D. Pi, R. Gresback, R. W. Liptak, S. A. Campbell, and U. Kortshagen, Appl. Phys. Lett. **92**, 123102 (2008).

[30] Z. Zhou, M. L. Steigerwald, R. A. Friesner, L. Brus, and M. S. Hybertsen, Phys. Rev. B **71**, 245308 (2005).

[31] G. Cantele, E. Degoli, E. Luppi, R. Magri, D. Ninno, G. Iadonisi, and S. Ossicini, Phys. Rev. B **72**, 113303 (2005).

[32] Q. Xu, J.-W. Luo, S.-S. Li, J.-B. Xia, J. Li, and S.-H. Wei, Phys. Rev. B **75**, 235304 (2007).

[33] T.-L. Chan, M. L. Tiago, E. Kaxiras, and J. R. Chelikowsky, Nano. Lett. **8**, 596 (2007).

[34] T.-L. Chan, H. Kwak, J.-H. Eom, S. B. Zhang, and J. R. Chelikowsky, Phys. Rev. B **82**, 115421 (2010).

[35] T.-L. Chan, S. B. Zhang, and J. R. Chelilowsky, Appl. Phys. Lett. **98**, 133116 (2011).

[36] J. Ma, S.-H. Wei, N. R. Neale, and A. J. Nozik, Appl. Phys. Lett. **98**, 173103 (2011).

[37] A. D. Yoffe, Adv. Phys. **50**, 1 (2001).

[38] H. Peelaers, B. Partoens, and F. M. Peeters, Nano Lett. **6**, 2781 (2006).

[39] E. Durgun, N. Akman, C. Ataca, and S. Ciraci, Phys. Rev. B **76**, 245323 (2007).

[40] R. Rurali, Rev. Mod. Phys. **82**, 427 (2010).

[41] W. Kohn and L. J. Sham, Phys. Rev. **140**, A1133 (1965).

[42] G. Kresse and J. Furthmuller, Phys. Rev. B **54**, 11169 (1996).

[43] G. Kresse and D. Joubert, Phys. Rev. B **59**, 1758 (1999).

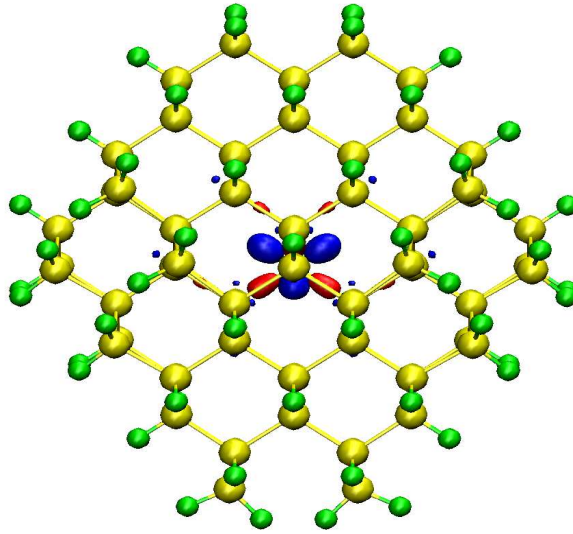[44] J. Li, S.-H. Wei, S.-S. Li, and J.-B. Xia, Phys. Rev. B **77**, 113304 (2008).

FIG. 1: The structure of the undoped Si QD. The charge densities of the HOMO and LUMO are also shown. Green balls represent H atoms, and yellow balls represent Si atoms. The charge density of the HOMO is in red, and that of the LUMO is in blue. They are both located at the center of the QD.
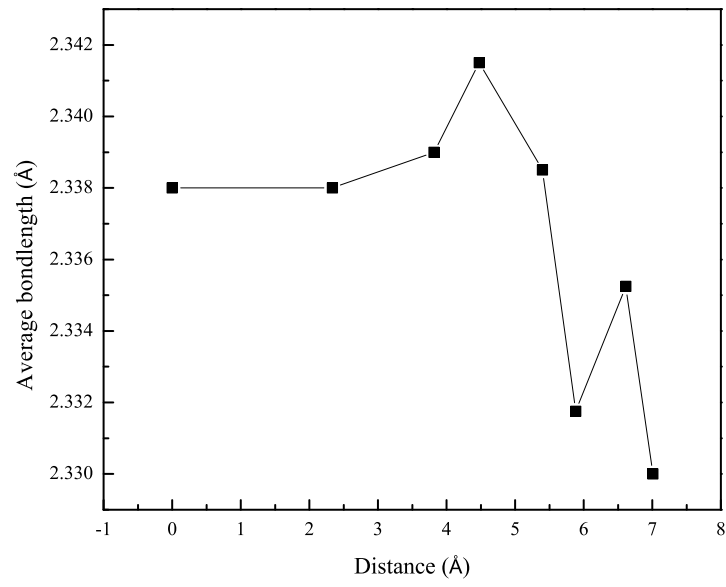
FIG. 2: The average bond length of the four Si-Si bonds at every non-equivalent site in the undoped Si QD. The x-axis is the distance between the site and the center of the QD. The bond length at the center of the Si QD (2.338 Å) achieves the bulk limit.
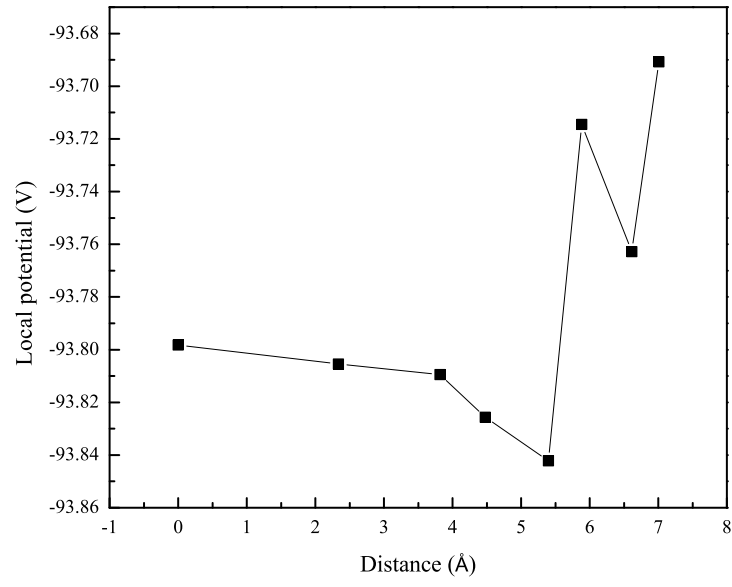
FIG. 3: The local potential at every non-equivalent site in the undoped Si QD. The x-axis is the distance between the site and the center of the QD.
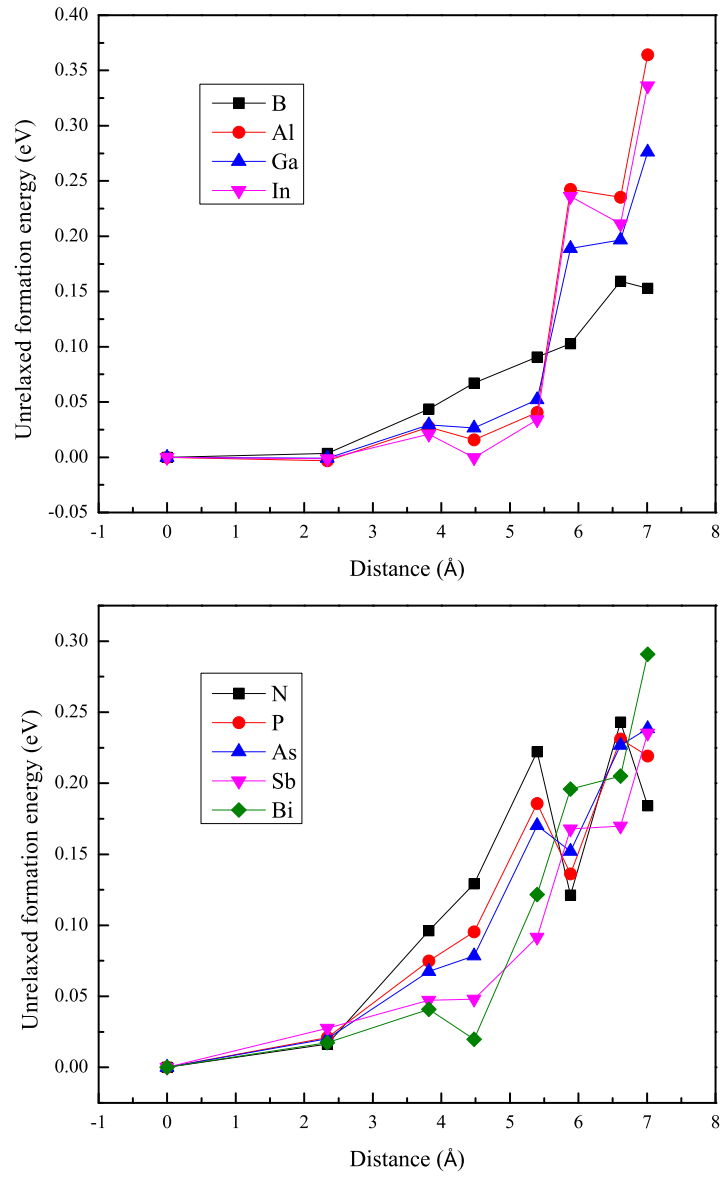
FIG. 4: The unrelaxed formation energies of various group-III acceptors (upper panel) and group-V donors (bottom panel) at every non-equivalent site. The x-axis is the distance between the dopant site and the center of the QD. The relaxation around the dopant is not considered here. For comparison, we set the unrelaxed formation energy of every dopant at the center site as zero.
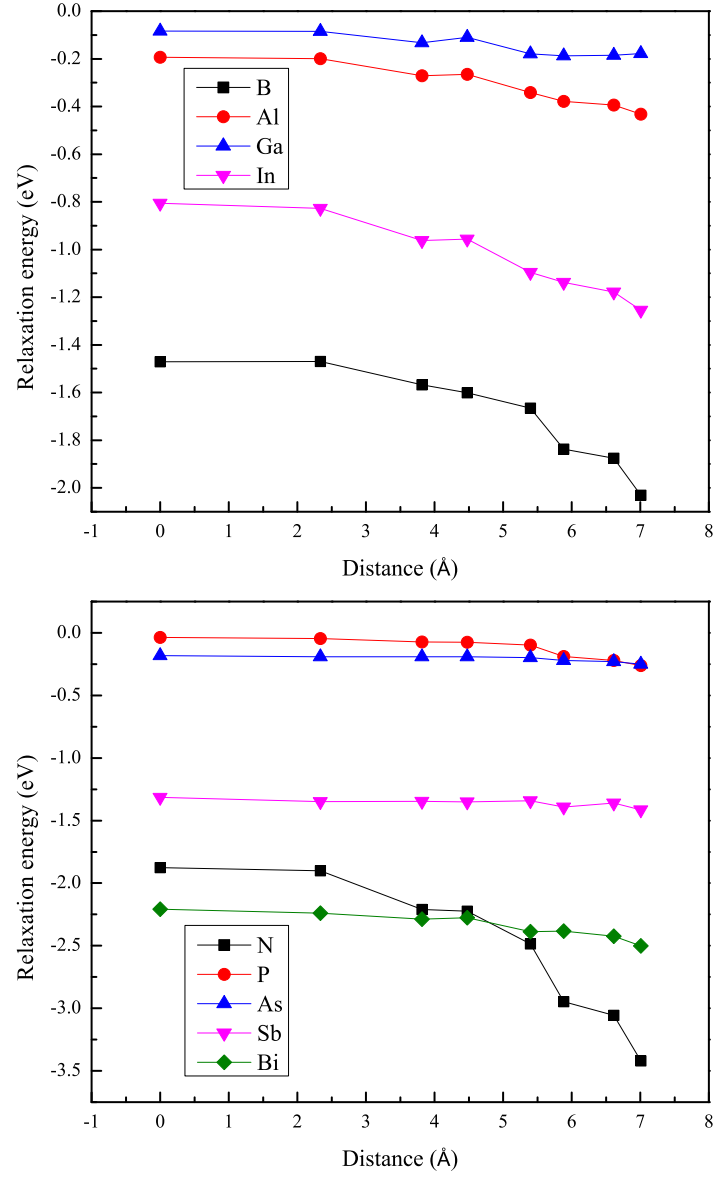
FIG. 5: The relaxation energies of various group-III acceptors (upper panel) and group-V donors (bottom panel) at every non-equivalent site. The x-axis is the distance between the dopant site and the center of the QD.
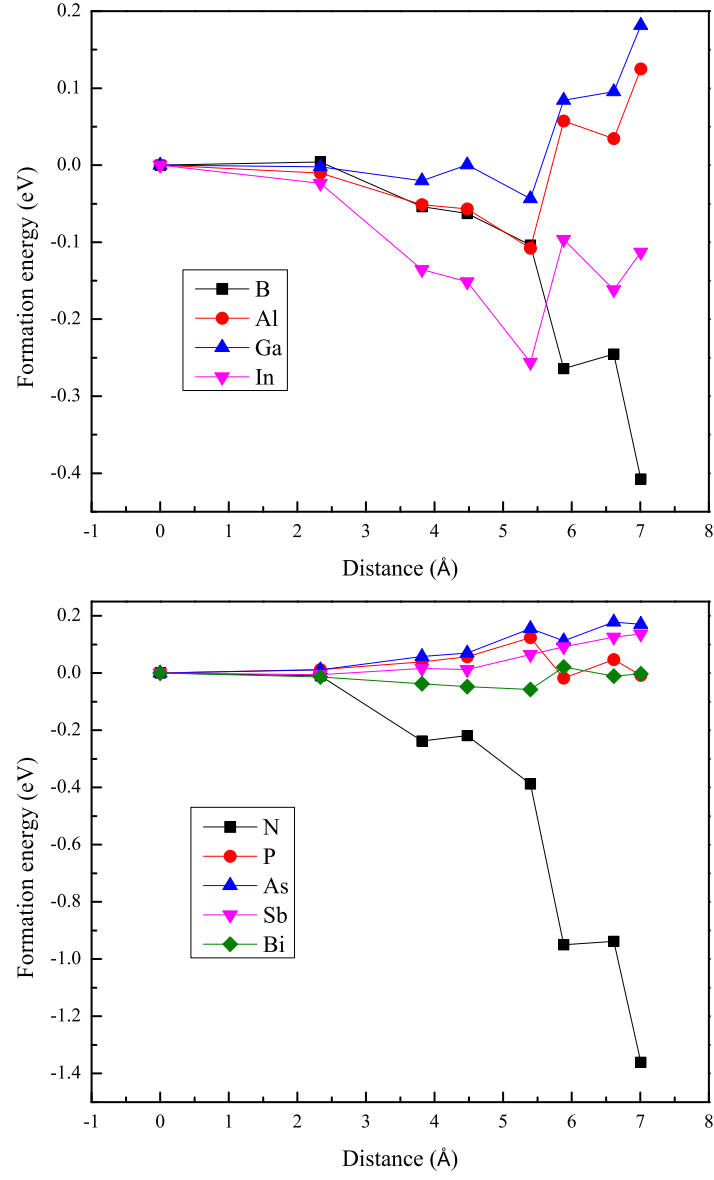
FIG. 6: The formation energies of various group-III acceptors (upper panel) and group-V donors (bottom panel) at every non-equivalent site. The x-axis is the distance between the dopant site and the center of the QD. For comparison, we set the formation energy of every dopant at the center site as zero.